

Adult restoration of *Shank3* expression rescues selective autistic-like phenotypes

Yuan Mei^{1*}, Patricia Monteiro^{1,2,3*}, Yang Zhou¹, Jin-Ah Kim¹, Xian Gao^{1,4}, Zhanyan Fu^{1,3} & Guoping Feng^{1,3}

Because autism spectrum disorders are neurodevelopmental disorders and patients typically display symptoms before the age of three¹, one of the key questions in autism research is whether the pathology is reversible in adults. Here we investigate the developmental requirement of *Shank3* in mice, a prominent monogenic autism gene that is estimated to contribute to approximately 1% of all autism spectrum disorder cases^{2–6}. SHANK3 is a postsynaptic scaffold protein that regulates synaptic development, function and plasticity by orchestrating the assembly of postsynaptic density macromolecular signalling complex^{7–9}. Disruptions of the *Shank3* gene in mouse models have resulted in synaptic defects and autistic-like behaviours including anxiety, social interaction deficits, and repetitive behaviour^{10–13}. We generated a novel *Shank3* conditional knock-in mouse model, and show that re-expression of the *Shank3* gene in adult mice led to improvements in synaptic protein composition, spine density and neural function in the striatum. We also provide behavioural evidence that certain behavioural abnormalities including social interaction deficit and repetitive grooming behaviour could be rescued, while anxiety and motor coordination deficit could not be recovered in adulthood. Together, these results reveal the profound effect of post-developmental activation of *Shank3* expression on neural function, and demonstrate a certain degree of continued plasticity in the adult diseased brain.

SHANK3 (also known as ProSAP2) protein is a major scaffolding protein at the excitatory synapse, coordinating the recruitment of many postsynaptic signalling molecules^{14,15}. Previous work has shown that germline deletion of *Shank3* in mice disrupts the protein composition at the postsynaptic density (PSD), reduces neurotransmission efficiency and leads to autistic-like behaviour^{10–13}.

To address whether adult reversal of physiological and behavioural abnormalities in *Shank3* mutant mice is possible, we adopted a genetic method that allows for inducible *Shank3* expression. Because *Shank3* duplication is linked to attention deficit hyperactivity disorder and bipolar disorder^{5,6,16}, it is crucial to keep *Shank3* expression within its physiological concentrations to avoid potential confounds. Thus, we generated a novel *Shank3* conditional knock-in mouse by using the Cre-dependent genetic switch (FLEX) strategy¹⁷, which enables the conditional manipulation of the *Shank3* gene at its endogenous genomic locus.

We genetically targeted the PDZ domain owing to its role in assembling the scaffold complex in the PSD^{14,15} (Fig. 1a and Extended Data Fig. 1). In the absence of Cre, the *Shank3^{flx/flx}* mice function as *Shank3* knockout (KO) mice, and result in the deletion of most major isoforms of SHANK3 including the putative α , β and γ bands (Fig. 1b). Similar to abnormalities previously reported on *Shank3* knockout mice^{10–13}, these *Shank3^{flx/flx}* mice showed significant deficits in exploratory behaviour (Fig. 1c), anxiety (Fig. 1e) and motor coordination (Fig. 1d), and

displayed open wound lesions that suggested repetitive grooming behaviour^{12,18}. In addition, they showed impaired neurotransmission in the dorsal striatum (Fig. 1f, g). These novel *Shank3^{flx/flx}* mice thus recapitulate autistic-like phenotypes, enabling us to investigate the possibility of reversing those deficits in adulthood.

To achieve temporal control of *Shank3* expression, we crossed the *Shank3^{flx/flx}* mice to an inducible CAGGS-CreER mouse line¹⁹ that activates global Cre function after tamoxifen treatment (Extended Data Fig. 1d). When the *Shank3^{flx/flx};CreER^{+/-}* mice reached 2–4.5 months, we used oral gavage to deliver tamoxifen to ensure efficient Cre-mediated gene restoration (Fig. 2a). All experiments were performed on the following three groups: *Shank3^{+/+};CreER^{+/-}* mice

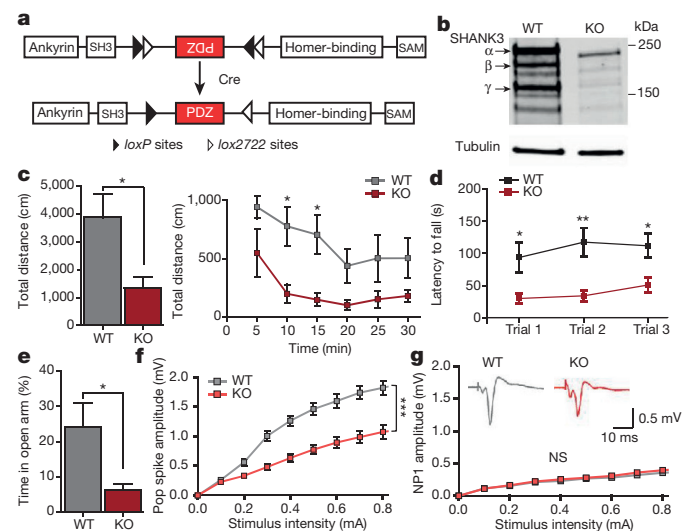


Figure 1 | *Shank3^{flx/flx}* mice have deficits in neurotransmission and behaviour. **a**, Domain structure of SHANK3 protein, with FLEXed PDZ domain inverted, which can be re-oriented in the presence of Cre. **b**, Western blot showing SHANK3 expression in striatal PSD from wild-type (WT) and *Shank3^{flx/flx}* (KO) mice. **c**, KO mice show decreased total distance travelled in the open-field test compared to WT mice. **d**, KO mice show impaired motor coordination in the rotarod test. **e**, KO mice spend less time in the open arm during the elevated zero maze test. **f**, KO mice show a decreased pop spike amplitude in extracellular field recordings in the striatum. **g**, Normal relationship of stimulation intensity to the negative peak 1 (NP1) amplitude (action potential component), suggesting unaltered presynaptic function; insets show representative traces. * $P < 0.05$, ** $P < 0.01$, *** $P < 0.001$ (two-tailed *t*-test (c, left, e) and two-way repeated measures analysis of variance (ANOVA) with Bonferroni post-hoc test (c, right, d, f, g)). Data are mean \pm s.e.m. (all behaviour data from $n = 6$ WT and $n = 7$ KO mice; electrophysiology data from $n = 9$ slices; 3 mice per genotype). See Supplementary Fig. 1 for gel source data.

¹McGovern Institute for Brain Research, Department of Brain and Cognitive Sciences, Massachusetts Institute of Technology, Cambridge, Massachusetts 02139, USA. ²PhD Programme in Experimental Biology and Biomedicine (PDBEB), Center for Neuroscience and Cell Biology, University of Coimbra, 3004-517 Coimbra, Portugal. ³Stanley Center for Psychiatric Research, Broad Institute of MIT and Harvard, Cambridge, Massachusetts 02142, USA. ⁴Key Laboratory of Brain Functional Genomics (Ministry of Education & Science and Technology Commission of Shanghai Municipality), Institute of Cognitive Neuroscience, School of Psychology and Cognitive Science, East China Normal University, Shanghai 200062, China.

*These authors contributed equally to this work.

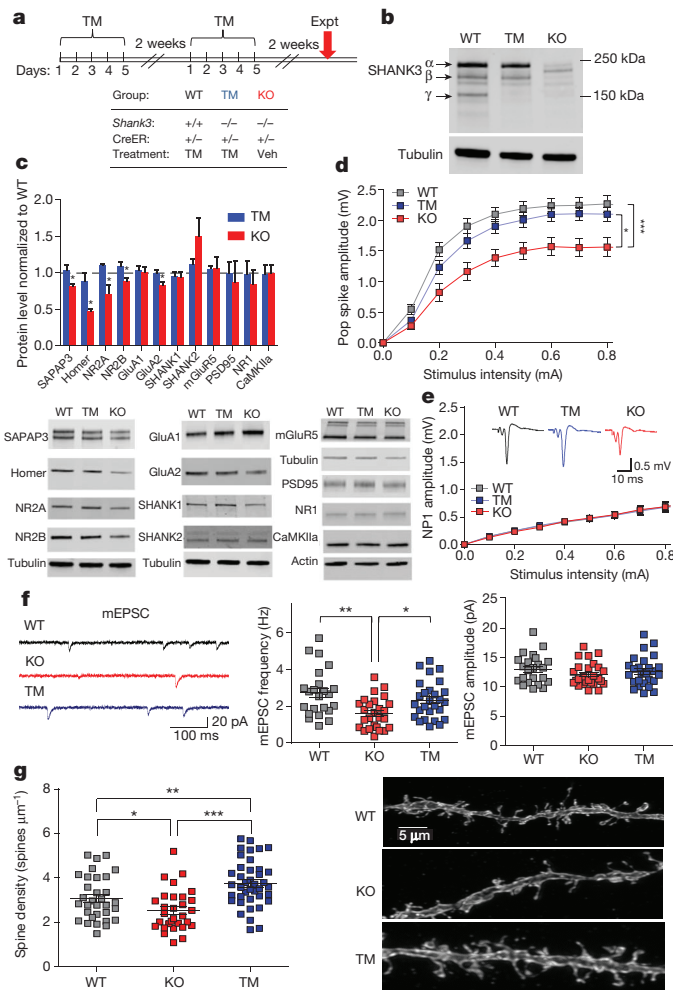


Figure 2 | Rescue of PSD proteins and striatal neurotransmission. **a**, Experimental groups and TM feeding scheme. Expt, experiment; veh, vehicle. **b**, Western blot from striatal synaptosome preparation after tamoxifen feeding shows restoration of most SHANK3 isoforms. **c**, Western blots of striatal synaptosomal fractions (bottom); PSD protein levels in KO mice are restored to WT levels in the TM group (top). **d**, Striatal field response in KO mice was rescued in TM mice. **e**, Representative traces for WT, KO and TM mice. Indistinguishable relationship of stimulation intensity to the NP1 amplitude among groups suggests unaltered presynaptic function. **f**, Rescued mEPSC frequency in the striatum in the TM compared to KO mice. **g**, Increased spine density in the TM compared to KO mice, while spine density in the KO mice is lower than that of the WT. * $P < 0.05$, ** $P < 0.01$, *** $P < 0.001$ (Student's two-tailed t -test (c), two-way repeated measures ANOVA with Bonferroni post-hoc test (d, e), one-way ANOVA with Bonferroni post-hoc test (f), one-way ANOVA with Newman–Keuls multiple comparison post-hoc test (g)). Data are mean \pm s.e.m. (c: $n = 3$ WT, $n = 4$ TM and $n = 3$ KO; each sample represents combined striatal tissue from 2 mice; d and e: $n = 12$ slices from 4 WT, 4 TM and 4 KO mice; f: $n = 23$ WT, $n = 26$ KO and $n = 27$ TM cells; g: $n = 32$ WT, $n = 30$ KO and $n = 40$ TM dendritic segments). See Supplementary Fig. 1 for gel source data.

treated with tamoxifen (wild type, WT), *Shank3^{fx/fx}:CreER^{+/-}* mice treated with tamoxifen (TM), and *Shank3^{fx/fx}:CreER^{+/-}* mice treated with corn oil vehicle (KO). Synaptosomal preparations showed that tamoxifen treatment restored the expression of most major SHANK3 isoforms, including the α and β isoforms, to the wild-type level at synapses (Fig. 2b).

Because SHANK3 is the only SHANK protein family member highly enriched in the striatum, a region strongly implicated in certain behaviours associated with autism^{12,18}, mechanistic characterizations were primarily carried out on striatal neurons. We found that the synaptic

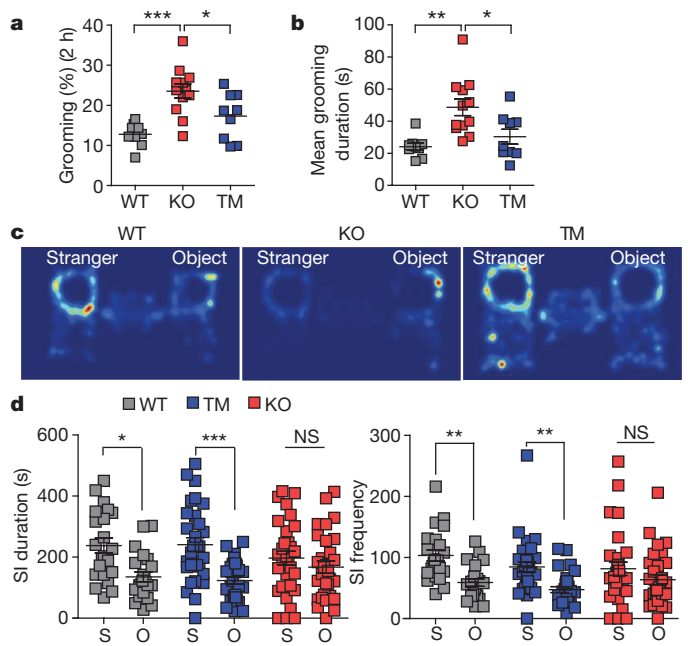


Figure 3 | Adult *Shank3* expression rescued repetitive grooming and social interaction. **a, b**, Significantly reduced repetitive grooming behaviour in TM compared to KO mice. **c**, Representative heat maps from the social interaction test for all groups. **d**, Unlike WT mice, KO mice showed no preference for social interaction (SI) with a stranger (S) mouse rather than a novel object (O); this behaviour is rescued in the TM group. * $P < 0.05$, ** $P < 0.01$, *** $P < 0.001$ (one-way repeated measures ANOVA with Bonferroni post-hoc test (a, b, d, left), Kruskal–Wallis test with Dunn's multiple comparison test owing to non-normal distribution (d, right)). Data are mean \pm s.e.m. (a and b: $n = 9$ WT, $n = 9$ TM and $n = 12$ KO mice; d: $n = 22$ WT, $n = 30$ TM and $n = 30$ KO mice).

concentrations of scaffold proteins SAPAP3, Homer1b/c and glutamate receptor subunits NR2A, NR2B and GluA2 were significantly reduced in KO striatal synaptosomal preparations. However, in the TM condition, the synaptic levels of these postsynaptic proteins were significantly increased compared to those in the KO mice, reaching comparable levels to the WT (Fig. 2c). This molecular alteration shows for the first time, to our knowledge, that restoring *Shank3* expression in the adult brain can efficiently recruit major scaffolding and signalling proteins to the synapse and assemble the PSD protein network even after the developmental period.

To investigate whether there were functional changes parallel to molecular repair at synapses, we examined striatal physiology. As expected, the KO mice showed significantly reduced field population spikes. However, the reduced field responses were rescued to WT levels in the TM condition (Fig. 2d, e). We then performed whole-cell recordings and found that the KO mice had reduced miniature excitatory postsynaptic current (mEPSC) frequency compared to WT mice. Notably, mEPSC frequency was rescued in the TM condition to comparable levels of the WT group (Fig. 2f). We also measured the paired-pulse ratio, the AMPAR/NMDAR ratio (α -amino-3-hydroxy-5-methyl-4-isoxazole propionic acid receptor/*N*-methyl-D-aspartate receptor) (Extended Data Figs 2 and 3), and NR2B (also known as GRIN2B)/total NMDAR ratio (Extended Data Fig. 2c). We found no differences across genotypes. Overall, these results suggest that a primary defect of striatal physiology in KO mice is the reduced mEPSC frequency, and this defect can be improved by restoring SHANK3 expression in adulthood.

Previous studies have shown that *Shank3* manipulation can lead to significant changes in the total spine density^{6,12}. It is, however, unclear whether post-developmental *Shank3* expression can also affect spine structure. To address this, we used systemic viral injection to sparsely label neurons with green fluorescent protein (GFP) in the WT, KO

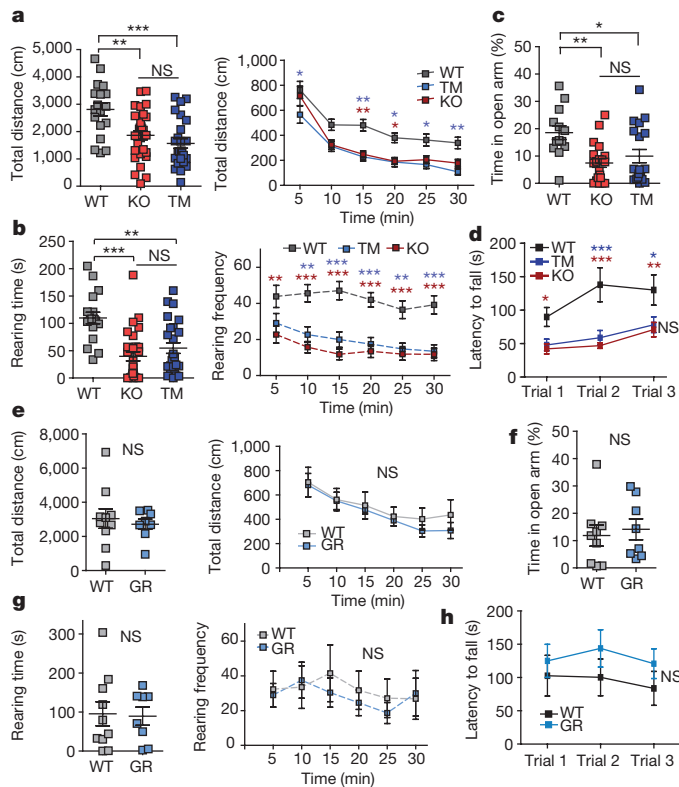


Figure 4 | Restoring *Shank3* expression in adulthood did not rescue anxiety and rotarod deficits. **a, b**, Open-field tests indicated that SHANK3 re-expression in adults (TM) does not rescue reduced locomotion and reduced rearing (axiogenic behaviour) in KO mice. NS, not significant. **c**, KO mice spend less time exploring the open arm during the elevated zero maze test; this behaviour is also not rescued in TM group. **d**, Motor coordination measurement from rotarod is not rescued in TM group. **e–h**, Germline rescued (GR) *Shank3^{fl/fl}* mice show that all above parameters for open-field, elevated zero maze and rotarod tests can be rescued if *Shank3* expression is restored at the germ-cell stage. * $P < 0.05$, ** $P < 0.01$, *** $P < 0.001$ (one-way ANOVA (a, left, c), Kruskal–Wallis test with Dunn’s multiple comparisons (b, left), two-tailed *t*-test (e, left, f, g, left); two-way repeated measures ANOVA with Bonferroni post-hoc test (a, right, b, right, d, e, right, g, right, h). Data are mean \pm s.e.m. (a–c: $n = 18$ WT, $n = 25$ TM and $n = 27$ KO mice; d: $n = 13$ WT, $n = 19$ TM and $n = 21$ KO mice; e–h: $n = 10$ WT and $n = 8$ GR mice).

and TM mice and analysed their dendritic spines in the dorsal striatum. Similar to our previous report on *Shank3B* (a *Shank3* isoform) KO mice¹², we observed a significant reduction of medium spiny neuron (MSN) spine density in the KO compared to WT mice. Surprisingly, the total spine density was significantly increased in the TM-treated mice compared to the KO mice (Fig. 2g). To our knowledge, this is the first indication that the ability of *Shank3* to promote spine formation or maintenance is not restricted to any developmentally critical period, highlighting the continued structural plasticity in the adult striatum. Interestingly, the spine density in the TM condition is significantly higher than that of the WT. One possibility for this phenomenon is that adult *Shank3* expression induces dendritic spines that may not be pruned and regulated by the same processes that occur in development.

We next tested how adult SHANK3 expression may affect behavioural abnormalities. Because striatal defects have been strongly linked to repetitive and compulsive behaviours^{20,21}, and *Shank3* KO mice show signs of overgrooming¹², we filmed WT, TM and KO mice after treatment, and quantified their grooming time. The results indicated that while there was a significant increase in the percentage of time spent grooming in the KO mice compared to WT mice, TM mice exhibited a significantly reduced grooming time (Fig. 3a, b). In addition, during the tamoxifen treatment, we noticed that some *Shank3^{fl/fl};CreER^{+/−}* mice

that had initially developed lesions began to heal and regrow their lost fur, providing further support that the repetitive/excessive grooming phenotype is reversible in the *Shank3^{fl/fl}* mice.

One of the defining features of autism is the impairment in social interaction. Thus, we used a modified three-chamber assay to probe voluntary social interaction^{12,13,22}. After habituating to the three-chamber box, the test mice were given a choice of interacting with either a novel object or a stranger mouse. We found that although WT mice demonstrated a strong preference for the stranger mouse compared with the novel object, KO mice displayed no such preference (Fig. 3c, d). Notably, we found that TM mice behaved similarly to the WT controls in that they showed a strong preference for the stranger mouse in both the duration and frequency of the interaction (Fig. 3c, d). These data show that, similar to the repetitive grooming behaviour, the social interaction deficit can also be rescued in adulthood. Currently, the neurobiological mechanisms of social deficits of autism spectrum disorder are not well understood. Although ventral striatum has been associated with social interaction²³, we did not observe differences in the measurements of mEPSCs, the AMPAR/NMDAR ratio or the paired-pulse ratio in the ventral striatum/nucleus accumbens across genotypes (Extended Data Fig. 4).

Encouraged by the rescue of repetitive grooming and social deficits, we ran a range of other tests to assess the extent of behavioural rescue. In contrast to the social and grooming behaviours, adult *Shank3* re-expression has minimal effect on reduced locomotion, anxiety-like behaviour and motor coordination deficits (Fig. 4). In the open-field test, TM mice showed no significant difference from the KO mice in exploratory behaviour (Fig. 4a) and anxiety-like behaviour including rearing time and rearing frequency (Fig. 4b). This result was further corroborated by our observations from the elevated zero maze test (Fig. 4c). In addition, we found no significant recovery in the motor coordination deficit (Fig. 4d).

Because the cortex and cerebellum have been linked to anxiety and motor coordination, we assessed the mechanistic changes in these brain regions^{24,25}. In both regions, SHANK3 expression was restored to the WT level in TM mice (Extended Data Figs 5 and 6). However, we found minimal differences across the genotypes (Extended Data Figs 5–7). Thus, the circuit mechanisms of anxiety and motor coordination deficits in the *Shank3* KO mice may involve other brain regions or could be the collective consequence of connectivity deficits across many brain regions.

To address whether the lack of rescue in these behaviour phenotypes is indeed due to missing SHANK3 expression during development, we crossed *Shank3^{fl/fl}* mice to β -actin-Cre mice, enabling germline restoration of *Shank3*. The germline rescue mice showed no significant differences in striatal physiology (Extended Data Figs 4 and 8), exploratory behaviour (Fig. 4e), anxiety (Fig. 4f, g) or motor coordination (Fig. 4h) compared to their wild-type littermates, indicating that restoring *Shank3* expression at the germ-cell stage can restore all behavioural phenotypes. Together, these data strongly suggest that there are certain developmental defects that are irreversible by adult re-expression of *Shank3*.

To test whether there is a developmental window for rescuing anxiety and motor deficits, we treated postnatal day (P) 20–21 mice with tamoxifen to induce *Shank3* expression efficiently (Extended Data Fig. 9a), and assayed their behaviours in adulthood (Extended Data Figs 9 and 10). As previously reported²⁶, we observed that the treatment of young mice with tamoxifen leads to some toxicity including reduced body weights in the wild-type mice, and affected their motor coordination compared to the KO mice fed with corn oil (Extended Data Fig. 10d). However, even with the TM toxicity, we found that on the rotarod, the developmentally treated TM mice performed significantly better than their KO counterparts (Extended Data Fig. 10a, b). The P20–P21-treated TM mice also showed significantly reduced anxiety on the elevated zero maze compared to the KO mice (Extended Data Fig. 9f). Overall, these behavioural results show that earlier intervention

yields more behavioural improvement than adult treatment, further supporting the developmental origin of the behavioural abnormalities that are irreversible in adults.

We have shown that in the adult mouse brain, *Shank3* expression can increase dendritic spine density, restore the PSD protein composition, and improve striatal neurotransmission. Although adult gene rescue characterizations have been performed on other autism genes^{27,28}, this is the first report, to our knowledge, to show selective rescue in specifically autism-related behavioural phenotypes. Notably, we also demonstrated that the behavioural deficits that are irreversible in the adult can be improved by early postnatal intervention. Our results highlight the unique behavioural effect of SHANK3 expression after development, and underscore the surprising extent of continued neural plasticity in the adult brain.

Online Content Methods, along with any additional Extended Data display items and Source Data, are available in the online version of the paper; references unique to these sections appear only in the online paper.

Received 5 January 2015; accepted 05 January 2016.

Published online 17 February 2016.

1. Amaral, D., Geschwind, D. & Dawson, G. *Autism Spectrum Disorders* 1st edn (Oxford Univ. Press, 2011).
2. Gauthier, J. *et al.* Novel *de novo* SHANK3 mutation in autistic patients. *Am. J. Med. Genet. B. Neuropsychiatr. Genet.* **150B**, 421–424 (2009).
3. El-Fishawy, P. & State, M. W. The genetics of autism: key issues, recent findings, and clinical implications. *Psychiatr. Clin. North Am.* **33**, 83–105 (2010).
4. Leblond, C. S. *et al.* Meta-analysis of SHANK mutations in autism spectrum disorders: a gradient of severity in cognitive impairments. *PLoS Genet.* **10**, e1004580 (2014).
5. Moessner, R. *et al.* Contribution of SHANK3 mutations to autism spectrum disorder. *Am. J. Hum. Genet.* **81**, 1289–1297 (2007).
6. Durand, C. M. *et al.* Mutations in the gene encoding the synaptic scaffolding protein SHANK3 are associated with autism spectrum disorders. *Nature Genet.* **39**, 25–27 (2007).
7. Ebert, D. H. & Greenberg, M. E. Activity-dependent neuronal signalling and autism spectrum disorder. *Nature* **493**, 327–337 (2013).
8. Kim, E. *et al.* GKAP, a novel synaptic protein that interacts with the guanylate kinase-like domain of the PSD-95/SAP90 family of channel clustering molecules. *J. Cell Biol.* **136**, 669–678 (1997).
9. Takeuchi, M. *et al.* SAPAPs. A family of PSD-95/SAP90-associated proteins localized at postsynaptic density. *J. Biol. Chem.* **272**, 11943–11951 (1997).
10. Wang, X. *et al.* Synaptic dysfunction and abnormal behaviors in mice lacking major isoforms of *Shank3*. *Hum. Mol. Genet.* **20**, 3093–3108 (2011).
11. Bozdagi, O. *et al.* Haploinsufficiency of the autism-associated *Shank3* gene leads to deficits in synaptic function, social interaction, and social communication. *Mol. Autism* **1**, 15 (2010).
12. Peça, J. *et al.* *Shank3* mutant mice display autistic-like behaviours and striatal dysfunction. *Nature* **472**, 437–442 (2011).
13. Yang, M. *et al.* Reduced excitatory neurotransmission and mild autism-relevant phenotypes in adolescent *Shank3* null mutant mice. *J. Neurosci.* **32**, 6525–6541 (2012).
14. Sheng, M. & Kim, E. The Shank family of scaffold proteins. *J. Cell Sci.* **113**, 1851–1856 (2000).
15. Boeckers, T. M. *et al.* Proline-rich synapse-associated proteins ProSAP1 and ProSAP2 interact with synaptic proteins of the SAPAP/GKAP family. *Biochem. Biophys. Res. Commun.* **264**, 247–252 (1999).
16. Han, K. *et al.* SHANK3 overexpression causes manic-like behaviour with unique pharmacogenetic properties. *Nature* **503**, 72–77 (2013).

17. Schnütgen, F. *et al.* A directional strategy for monitoring Cre-mediated recombination at the cellular level in the mouse. *Nature Biotechnol.* **21**, 562–565 (2003).
18. Karayannis, T. *et al.* Cntnap4 differentially contributes to GABAergic and dopaminergic synaptic transmission. *Nature* **511**, 236–240 (2014).
19. Guo, C., Yang, W. & Lobe, C. G. A Cre recombinase transgene with mosaic, widespread tamoxifen-inducible action. *Genesis* **32**, 8–18 (2002).
20. Rothwell, P. E. *et al.* Autism-associated neuroigin-3 mutations commonly impair striatal circuits to boost repetitive behaviors. *Cell* **158**, 198–212 (2014).
21. Welch, J. M. *et al.* Cortico-striatal synaptic defects and OCD-like behaviours in Sapap3-mutant mice. *Nature* **448**, 894–900 (2007).
22. Chao, H.-T. *et al.* Dysfunction in GABA signalling mediates autism-like stereotypies and Rett syndrome phenotypes. *Nature* **468**, 263–269 (2010).
23. Dölen, G. *et al.* Social reward requires coordinated activity of nucleus accumbens oxytocin and serotonin. *Nature* **501**, 179–184 (2013).
24. Gross, C. *et al.* Serotonin1A receptor acts during development to establish normal anxiety-like behaviour in the adult. *Nature* **416**, 396–400 (2002).
25. De Zeeuw, C. I. & Ten Brinke, M. M. Motor learning and the cerebellum. *Cold Spring Harb. Perspect. Biol.* **7**, a021683 (2015).
26. Poirier, M. C. & Schild, L. J. The genotoxicity of tamoxifen: extent and consequences, Kona, Hawaii, January 23, 2003. *Mutagenesis* **18**, 395–399 (2003).
27. Guy, J., Gan, J., Selfridge, J., Cobb, S. & Bird, A. Reversal of neurological defects in a mouse model of Rett syndrome. *Science* **315**, 1143–1147 (2007).
28. Clement, J. P. *et al.* Pathogenic SYNGAP1 mutations impair cognitive development by disrupting maturation of dendritic spine synapses. *Cell* **151**, 709–723 (2012).

Supplementary Information is available in the online version of the paper.

Acknowledgements We thank T. Dalia, A. Lim, S. Feng, K. Han, W. Stockton, H. Zaniewski and B. Clear for technical support. We thank Q. Zhang for designing the pAAV-hSYN1-EGFP-P2A-EGFPf-WPRE-HGHpA construct. We thank all members of the Feng laboratory for their support and discussions. Y.M. would like to thank T. Littleton, Y. Lin and K. Tye. P.M. would like to thank C. Duarte and the late S. Chatterjee, and acknowledge support from the ‘Programa Doutoral em Biologia Experimental e Biomedicina’ (CNC, Coimbra, Portugal). This work was funded by the National Science Foundation Graduate Fellowship and Integrative Neuronal Systems to Y.M.; the Stanley Center for Psychiatric Research at the Broad Institute of MIT and Harvard and a doctoral fellowship from the Portuguese Foundation for Science and Technology to P.M. (SFRH/BD/33894/2009). Y.Z. is supported by postdoc fellowships from the Simons Center for the Social Brain at MIT, Nancy Lurie Marks Family Foundation and Shenzhen Overseas Innovation Team Project (no. KQTD20140630180249366). X.G. was supported by the Stanley Center for Psychiatric Research at the Broad Institute of MIT and Harvard and a graduate fellowship from China Scholarship Council. Z.F. is supported by Stanley Center for Psychiatric Research at Broad Institute of MIT and Harvard and NARSAD Young Investigator Grant from the Brain & Behavior Research Foundation. Research in the Feng laboratory is supported by the Poitras Center for Affective Disorders Research at MIT, Stanley Center for Psychiatric Research at Broad Institute of MIT and Harvard, National Institute of Health (NIMH R01MH097104), Nancy Lurie Marks Family Foundation, Simons Foundation Autism Research Initiative (SFARI) and Simons Center for the Social Brain at MIT.

Author Contributions Y.M., P.M. and G.F. designed the experiments and wrote the paper. Y.M., P.M., Y.Z., J.-A.K., X.G. and Z.F. performed the experiments and analysed the data. Y.M., P.M., Y.Z., J.-A.K., X.G. and Z.F. interpreted the results.

Author Information Reprints and permissions information is available at www.nature.com/reprints. The authors declare no competing financial interests. Readers are welcome to comment on the online version of the paper. Correspondence and requests for materials should be addressed to G.F. (fengg@mit.edu).

METHODS

Generation of *Shank3* conditional knock-in (*fx/fx*) mice. The *Shank3^{fx/fx}* targeting vector was designed by inverting the PDZ domain (exons 13–16) and flanking it with the FLEX cassette, which is composed of one pair of *loxP* sites staggered with one pair of *lox2722* sites. *Shank3^{fx/fx}* conditional knock-in mice were generated by homologous recombination in R1 embryonic stem cells and implanting the correctly targeted cells into C57 blastocysts using standard procedures. Correct locus insertion of the targeting construct into the genomic DNA was determined by PCR genotyping using two primers End_F (5'-GGCAGACTCCACACAGTTCCTG-3') and LoxR (5'-GTATCCTATACGAAGTTATCCGGGTCGAC-3'). Subsequent mouse genotyping was determined by PCR of mouse tail or ear DNA using three primers. For the WT allele, primer FuncF2 (5'-CGTTTGACACACATAAGCACC-3') and primer FuncFlipR4 (5'-CTCCACCTAGCTGAATTTCCC-3') were used to produce a band of 340 base pairs (bp). For the knockout (Fx) allele, primer FuncF2 (5'-CGTTTGACACACATAAGCACC-3') and primer Gen_Flx_R1 (5'-GCTGACATCACATTGCTGCC-3') were used to produce a band of 481 bp. For the rescue allele, primer FuncF2 (5'-CGTTTGACACACATAAGCACC-3') and primer FuncFlipR4 (5'-CTCCACCTAGCTGAATTTCCC-3') were used to produce a band of 408 bp.

Chimaeric males were crossed to C57BL/6J females from Jackson Labs. The F₁ hybrids were crossed with C57BL/6J β -actin F1p to remove the neomycin cassette. All progeny were bred onto the pure C57BL/6J (Jackson Labs) for at least two generations before being bred onto a mixed background with 129S1/SvImJ (Jackson Labs). Heterozygotes were initially bred with heterozygotes to produce experimental animals. All germline *Shank3^{fx/fx}* (KO) and germline rescue (GR) mice along with their respective wild-type littermates were produced by breeding heterozygotes with heterozygotes. For the adult *Shank3* rescue experiments, the *Shank3* conditional knock-in line was crossed with CAGGS-CreER¹⁹. To produce enough animals for all necessary experiments, breeding strategy was switched to heterozygotes crossed with homozygotes and homozygotes crossed with homozygotes for all conditions (*Shank3^{fx/+}:CreER^{+/-}* bred with *Shank3^{fx/fx}:CreER^{-/-}*; *Shank3^{fx/fx}:CreER^{+/-}* bred with *Shank3^{fx/fx}:CreER^{-/-}*; *Shank3^{+/+}:CreER^{+/-}* bred with *Shank3^{+/+}:CreER^{-/-}*; *Shank3^{+/-}:CreER^{+/-}* bred with *Shank3^{+/+}:CreER^{-/-}*). It should be noted that all animals in the rescue condition were produced from the same litters as the animals in the knockout condition. The animals were randomly assigned to different conditions. No computerized randomization program was used.

Animals were housed by genotype at a constant 23°C in a 12-h light/dark cycle (lights on at 07:00, lights off at 19:00) with ad libitum food and water. Rescue treatment, that is tamoxifen feeding, was initiated on mice at 2–4.5 months. All electrophysiological and behavioural experiments were done at least 6 weeks after treatment in adult mice with the experimenter being blinded to the genotypes. Only age-matched male mice were used for behavioural assays. All experimental procedures were inspected and approved by the MIT Committee on Animal Care. **Open-field test.** An automated Omnitech Digiscan apparatus (AccuScan Instruments) was used to assess spontaneous locomotion as previously described²¹. Anxiety-like behaviours were assessed with the following parameters: time spent rearing and frequency of rearing. Locomotion was evaluated by the total distance travelled. The first 30 min were evaluated for all parameters. Statistical analysis was done using one-way ANOVA with Bonferroni multiple comparison tests.

Elevated zero maze test. An elevated zero maze was illuminated such that the open arm was lit by 60 Lx, and the dark arm was lit by 10–20 Lx. Animals were habituated with 10–20 Lx for at least 1 h before the test. The animal was introduced into the closed arm and allowed to explore the maze freely for 5 min, and this was filmed. An observer blinded to the genotype performed analysis using the automated tracking software Noldus Ethovision. Anxiety-like behaviour was assessed as the percentage of time spent by the animal in the open arm during the 5-min interval. Statistical analysis was done using one-way ANOVA with Bonferroni multiple comparison tests.

Rotarod test. Animals were placed on a rotarod apparatus (Med Associates) that accelerates 4–40 r.p.m. for 5 min. Each animal was tested for three trials with 1–2 h between trials in a single day. All trials were filmed. Latency to fall was manually analysed for each trial using Noldus Observer software by an observer blinded to genotypes. The change in the latency to fall over the course of three trials indicates the quality of motor coordination. Statistical analysis was done using two-way repeated measures ANOVA with Bonferroni post-hoc tests.

Grooming. Animals were individually placed into a new cage and allowed to habituate. Grooming behaviour was filmed for 2 h from 19:00 to 21:00 with red light (2 Lx). An observer blinded to the genotype manually quantified grooming behaviour using Noldus Observer. All instances of face-wiping, scratching/rubbing of head and ears, and full-body grooming were counted as grooming behaviour. Statistical analysis was done using one-way ANOVA with Bonferroni multiple comparison tests.

Social interaction test. A modified version of the three-chamber social interaction assay was used as previously described^{12,13,22}. Only age-matched males were used for all tests. S129 males were used as stranger mice and were habituated to the test chamber for three sessions (20 min each), 1 or 2 days before the behavioural assay. On the day of the test, both test and stranger animals were habituated to the test room for at least 1 h before the start of the assay. The left and right chambers of the three-chamber apparatus were both lit by 4–6 Lx during the test session. Each test animal was first placed into the centre chamber with open access to both the left and right chamber, each of which contained an empty wired cup placed upside down. This allowed the animal to habituate to not only the social apparatus, but also to the cups that will eventually contain the stranger mice. After 15 min of habituation, the test animal was moved back to the centre chamber briefly before the next session. During the social phase, an age-matched stranger mouse was placed randomly into one of the two side chambers while a novel object was placed into the other side chamber. The test animal was allowed to explore the social apparatus freely and demonstrate whether it prefers to interact with the novel object or novel mouse. This social phase was also for 15 min. The placement of the stranger mouse and the object was alternated between test mice to eliminate any confounds due to chamber bias. Time spent by the test animal in close proximity (~5 cm) to the cup containing either the stranger or the object was calculated. Analysis was done by an observer blinded to the genotype on Noldus Ethovision. One-way ANOVA with Bonferroni post-hoc test was used for statistical analysis.

Tamoxifen preparation and feeding. Tamoxifen (Sigma, T5648) was dissolved in corn oil at 20 mg ml⁻¹ by vortexing. Freshly prepared tamoxifen was protected from light by aluminium foil and kept for 2–3 days at room temperature. Animal feeding needles from Harvard Apparatus (52-4025) were used for oral gavage. To avoid toxicity of tamoxifen, the following dosages were used for adult animals: mice at 17–21 g body weight were fed 5 mg day⁻¹; mice at 22–25 g body weight were fed 6 mg day⁻¹; mice at 26–29 g body weight were fed 7 mg day⁻¹; mice at 30–35 g body weight were fed 8 mg day⁻¹.

The adult animals were fed for 5 consecutive days followed by 2 weeks of rest. The animals were then fed for 5 more consecutive days followed by another 2 weeks of rest. Corn oil was used as a control. The mice fed with tamoxifen and with corn oil were housed separately to avoid contamination.

For induction of SHANK3 expression in P20–P21 animals, mice that weighed 7–9 g received 0.1 ml tamoxifen or corn oil per day for 2–3 consecutive days. Mice that weighed 10–12 g received 0.15 ml tamoxifen or corn oil per day for 2–3 consecutive days.

Western blot. PSD and synaptosomal fractions of the striatum, cortex and cerebellum were prepared as previously described²¹. Purified fractions were separated on SDS-PAGE and quantified using Odyssey Licor. β -Actin and tubulin were used as loading controls. Specific primary antibody for SAPAP3 was prepared as previously described²¹. Commercial antibodies used include SHANK3 (Santa Cruz, SC-30193), GluR1 (Millipore, MAB2263), GluR2 (Neuromab, 75-002), NR1 (BD Biosciences, 556308), NR2A (Millipore, 07-632), NR2B (Millipore, 05-920), Homer1 (Chemicon, AB5877, Synaptic Systems, 160022), Homer3 (Synaptic Systems, 160303), mGLUR5 (Abcam, ab76316), CaMKIIa (Millipore, 05-532), SHANK1 (Synaptic Systems, 162002), SHANK2 (Cell Signaling, 12218S), β -actin (Sigma, A5441) and tubulin (Sigma, T5168). Statistical analysis was done using two-tailed Student's *t*-tests.

Dendritic spine analysis. Age-matched male mice from WT ($n = 5$), KO ($n = 4$), 1 had to be euthanized owing to lesion development) and TM ($n = 5$) conditions at 6–12 months old were used. The pAAV-hSYN1-EGFP-P2A-EGFPf-WPRE-HGHpA construct was cloned and sent for commercial viral packaging by Upenn Viral Core with serotype 2/9. Farnesylated GFP (GFPf) was previously shown to target the membrane²⁹. To achieve sparse labelling, ~8–30 μ l of this virus with titre of 4.04×10^{13} genome copies (GC) ml⁻¹ was injected through the retro-orbital route into each mouse. Three weeks after viral injection, the mice were transcardially perfused with 4% paraformaldehyde and sectioned into 200- μ m slices. Immunohistochemistry was performed by staining the slices with an anti-GFP antibody (Invitrogen, A11122) for 48 h and 24 h of secondary antibody incubation. The stained slices were then surrounded by a 240- μ m depth spacer (Electron Microscopy Sciences) and mounted with Vectashield Mounting Media.

Confocal images were taken with a $\times 60$ objective of the dorsal striatum. Spine count on intact neurons began 30–40 μ m away from the soma and was extended for 10–60 μ m from the origin. Spine density was analysed automatically by Neuron Studio. All virus injections, imaging and software analysis were done with the experimenter blinded to the mouse genotypes. Statistical analysis was done using one-way ANOVA, Newman-Keuls post-hoc test.

Electrophysiology slices, dorsal and ventral striatum. Acute striatal slices were prepared from 3–7-month-old age-matched mice. Animals were anaesthetized by avertin intraperitoneal injection (tribromoethanol, 20 mg ml⁻¹, 0.5 mg g⁻¹ body weight) and transcardially perfused with ice-cold oxygenated NMDG-based

cutting aCSF solution (mM): 92 *N*-methyl-D-glucamine (NMDG), 2.5 KCl, 1.20 Na₄PO₄, 30 NaHCO₃, 20 HEPES, 25 glucose, 2 thiourea, 5 Na-ascorbate, 3 Na-pyruvate, 0.5 CaCl₂ and 10 MgSO₄ (~300 mOsm, 7.2–7.4 pH). After decapitation, brains were removed for sectioning in the same ice-cold cutting aCSF using a Vibratome 1200S (Leica Microsystems). For all dorsal striatal recordings, 300- μ m coronal slices were prepared, unless otherwise stated (Extended Data Fig. 3). For all nucleus accumbens (NAc) core recordings, 300- μ m parasagittal slices were prepared and NAc core was identified by the presence of anterior commissure. Slices were recovered in the same cutting aCSF solution at 32 °C for 12 min and transferred to room-temperature carbogenated regular aCSF (mM): 119 NaCl, 2.5 KCl, 1.2 NaH₂PO₄, 24 NaHCO₃, 12.5 glucose, 2 MgSO₄·7H₂O and 2 CaCl₂·2H₂O (~300 mOsm, 7.2–7.4 pH). Slices were allowed to recover at least \geq 1 h and transferred to a recording chamber (RC-27L, Warner Instruments) before recordings. Stimulations were performed using a platinum iridium concentric bipolar electrode (CBAPC75, FHC). For dorsolateral striatum coronal slices, electrode was placed at the corpus callosum to mainly stimulate corticostriatal axons. For dorsolateral striatum parasagittal slices, stimulating electrode was placed at the cortex between layer V and VI. For ventral striatum parasagittal slices, electrode was placed dorsally to the anterior commissure at the border between NAc core and the cortex. Afferents were stimulated with 0.1 ms stimulation step (Isoflex, AMPI) delivered at 0.05 Hz frequency (unless otherwise stated). Slices were visualized under IR-DIC (infrared-differential interference contrast) using a BX-51WI microscope (Olympus). All slice preparations, recordings and data analysis were performed with experimenter blinded to the genotypes.

Medial prefrontal cortex. Acute brain slices were prepared from 3–7-month-old mice as follows. In brief, mice were deeply anaesthetized by intraperitoneal injection of avertin solution (20 mg ml⁻¹, 0.5 mg g⁻¹ body weight) and then transcardially perfused with 20 ml of carbogenated (95% O₂, 5% CO₂) ice-cold cutting solution with the composition (in mM): 105 NMDG, 105 HCl, 2.5 KCl, 1.2 NaH₂PO₄, 26 NaHCO₃, 25 glucose, 10 MgSO₄, 0.5 CaCl₂, 1 L-ascorbic acid, 3 sodium pyruvate and 2 thiourea (pH 7.4, with osmolarity of 300–310 mOsm). The brains were rapidly removed and placed in ice-cold and oxygenated cutting solution. Coronal slices (300 μ m) were sliced using Leica VT1200S (Leica Microsystems) and then transferred to recovery chamber at 32 °C with carbogenated cutting solution for 8 min, followed by transferring to holding chamber containing aCSF that contained (mM): 119 NaCl, 2.3 KCl, 1.0 NaH₂PO₄, 26 NaHCO₃, 11 glucose, 1.3 MgSO₄ and 2.5 CaCl₂ (pH was adjusted to 7.4 with HCl, with osmolarity of 300–310 mOsm) at room temperature. Slices were allowed to recover for at least 2 h in holding chamber before recording and used for experiment typically between 3 and 7 h after slicing. Layer 5 pyramidal cells with a prominent apical dendrite were visually identified with a microscope equipped with IR-DIC optics (BX-51WI, Olympus) mainly by location, shape and pClampex online membrane test parameters.

Extracellular field recordings. Slices were prepared from a daily group of mice containing all the three genotypes/treatments on randomized order, and recordings were obtained at room temperature with carbogenated regular aCSF (~2 ml min⁻¹ rate). Borosilicate glass recording microelectrodes (King Precision Glass) were pulled on a P-97 horizontal puller (Sutter Instruments) and backfilled with 2 M NaCl. Recording electrode was placed ~400 μ m away from stimulating electrode and field population-spike was evoked by a 0.1 ms stimulation step (Isoflex, AMPI) delivered at 0.05 Hz frequency. Input–output functions were generated through consecutive rounds from 0.1–1.0 mA in 0.1 mA increments (triplicate measurements per stimulation intensity). Three components were resolved in the recording traces: stimulation artefact, negative peak 1 (NP1, presynaptic fibre volley) and field population spike. Amplitude for each component was determined by the average peak amplitude from triplicated measurements per stimulation intensity. Data were amplified using a MultiClamp 700B and sampled at 10 kHz using a Digidata 1440A acquisition system. Analysis was performed blinded to genotype using pCLAMP 10 software (Axon Instruments/Molecular Devices).

Whole-cell recordings. Borosilicate glass recording microelectrodes (King Precision Glass) were pulled on a P-97 horizontal puller (Sutter Instruments)

and backfilled with CsGlu (mM): 110 CsOH, 110 D-gluconic acid, 15 KCl, 4 NaCl, 5 TEA-Cl, 20 HEPES, 0.2 EGTA, 5 lidocaine *N*-ethyl chloride, 4 MgATP and 0.3 NaGTP. Internal pH was adjusted to ~7.3 with KOH and osmolarity adjusted to ~300 mOsm with K₂SO₄. Typical internal resistance was around 3–5 M Ω . MSNs were visually identified based on their shape, size and location under IR-DIC, using a BX-51WI microscope (Olympus). After seal rupture and internal equilibrium (5 min to allow proper dialysis of Cs⁺ internal), cells were recorded with series-resistance values <20 M Ω (recording traces were excluded for data analysis if series resistance changed by >20%). All voltage clamp traces were recorded in the presence of 50 μ M picrotoxin (Tocris) with theoretical liquid junction potential not corrected for. Signals were filtered at 2 kHz, digitized at 10 kHz and data acquired using a MultiClamp 700B amplifier and a Digidata 1440A. All analyses were performed blinded to the genotype. Grubb's test was used to remove single outliers.

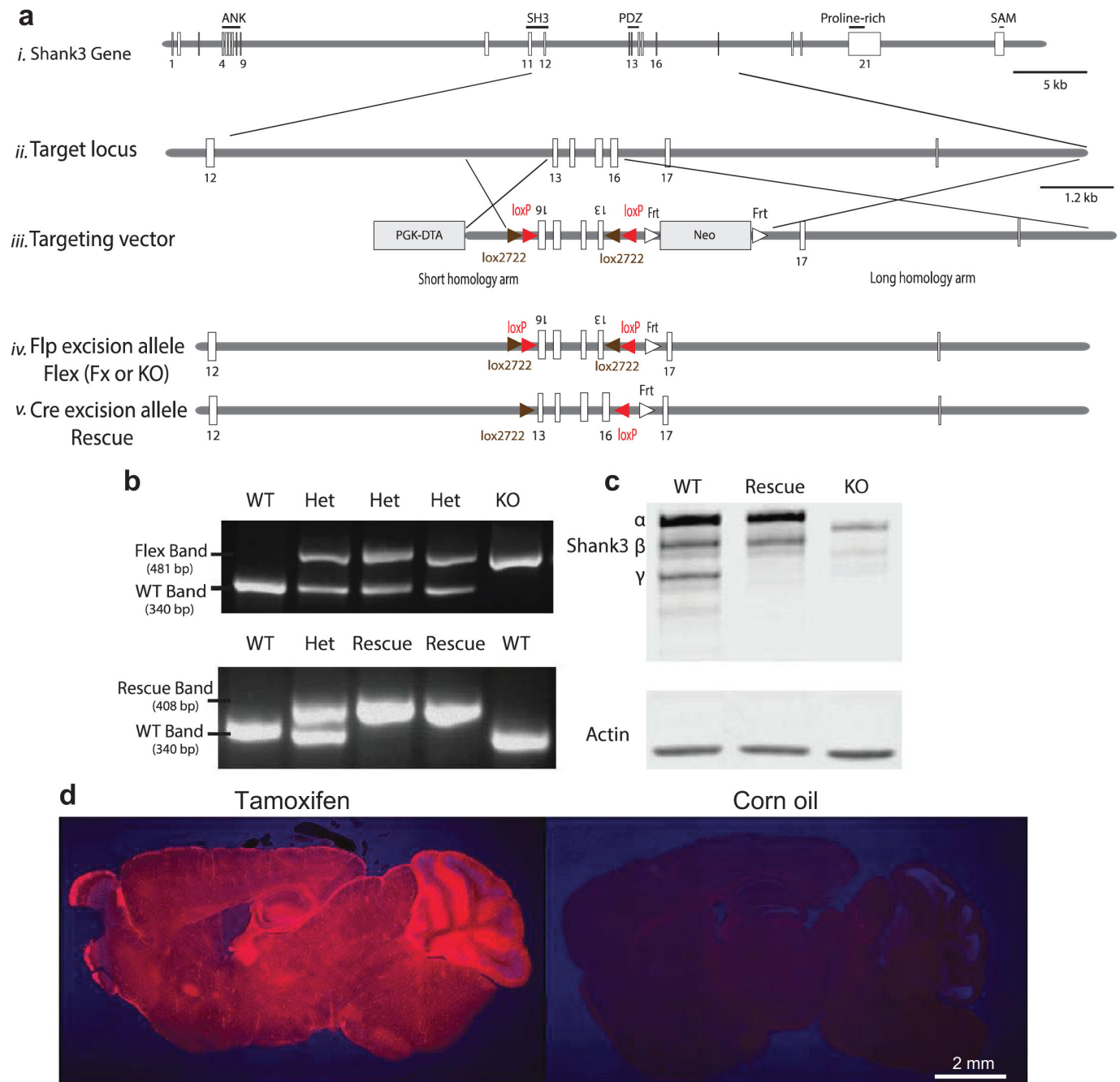
mEPSCs. Slices were perfused with room temperature carbogenated regular aCSF at a rate of approximately 2 ml min⁻¹. Voltage clamp traces were recorded at holding potential –70 mV in the presence of 50 μ M picrotoxin (Tocris), 50 μ M DL-AP5 (DL-2-amino-5-phosphonovaleric acid, Abcam) and 1 μ M tetrodotoxin (Tocris). Analysis of mEPSCs was performed using pCLAMP10 (Axon Instruments, Molecular Devices) and MiniAnalysis software (Synaptosoft) by manually clicking of individual events.

Paired-pulse ratios. Slices were perfused with carbogenated regular aCSF at ~30 °C, ~2 ml min⁻¹ rate. Stimulus intensity was set to evoke 150–400 pA EPSCs at holding potential –70 mV. Two EPSCs (inter-stimulus interval of 50 ms) were evoked for 10 consecutive traces. The paired-pulse ratio was calculated by dividing the second EPSC peak amplitude by the first one.

AMPA/NMDAR ratios. Slices were perfused with carbogenated regular aCSF at ~30 °C, ~2 ml min⁻¹ rate. Stimulus intensity was set to evoke 150–400 pA EPSCs at holding potential –70 mV. An average EPSC was obtained (~10 traces) at –70 mV and then at +40 mV. The AMPAR/NMDAR ratio was calculated as the ratio of the average EPSC peak amplitude at –70 mV (AMPA EPSC) to the average amplitude of the EPSC recorded at +40 mV, 50 ms after afferent stimulation. For pharmacologically isolated AMPAR/NMDAR ratios, dual-component evoked EPSCs at +40 mV was recorded before and after DL-AP5 bath application (50 μ M, Abcam). NMDAR EPSC was obtained by digitally subtracting the average EPSC amplitude after DL-AP5 application (AMPA EPSC). For NR2B/total NMDAR ratio, dual-component evoked EPSC at +40 mV was recorded before and after ifenprodil bath application (3 μ M, NR2B antagonist, Tocris) and ifenprodil blockable fraction was defined as NR2B EPSCs. DL-AP5 (50 μ M) was then applied to block all NMDARs for measuring total NMDAR EPSCs. The fraction of NR2B containing NMDAR EPSCs is presented as the percentage of the total NMDAR EPSCs (NR2B/total NMDAR ratio = ifenprodil sensitive current divided by DL-AP5 sensitive current).

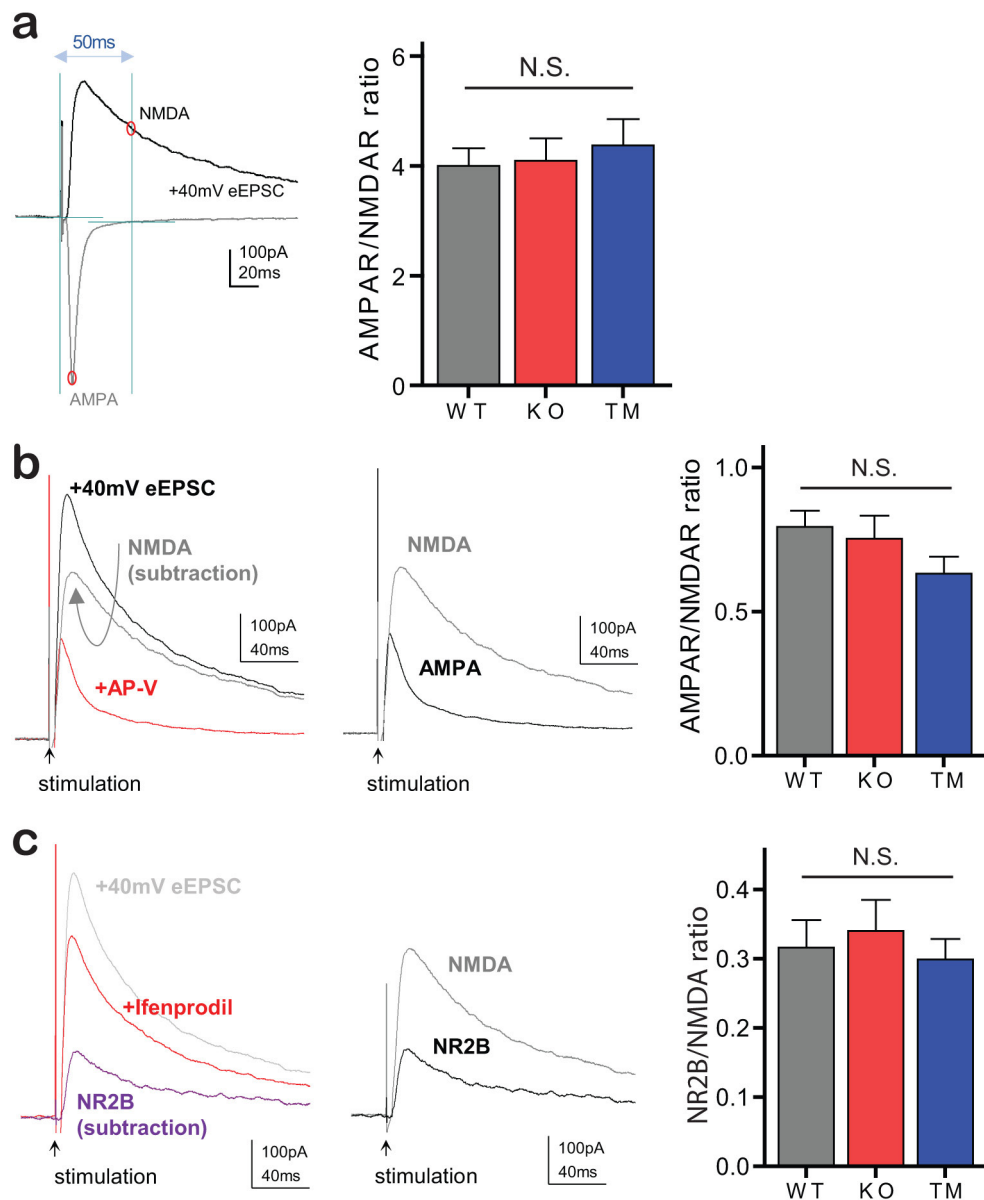
Statistical analyses. All statistical analyses were performed using Prism (GraphPad Software). All data sets were analysed using D'Agostino–Pearson omnibus test and Shapiro–Wilk test for normality. Data sets with normal distributions were analysed for significance using either unpaired Student's two-tailed *t*-test or ANOVA measures with multiple comparison post-hoc test, using **P* < 0.05, ***P* < 0.01, ****P* < 0.001; all data presented as mean \pm s.e.m. Data sets with non-normal distributions were analysed using Kruskal–Wallis test with adjustments for multiple comparisons. On the basis of previously published SHANK3 models^{10–13}, we chose similar sample sizes for all experiments performed. All behaviour test results for the tamoxifen-treated cohorts are the combination of at least two different large animal cohorts that showed the same results. All electrophysiological, biochemical and morphological data were obtained by counterbalancing experimental conditions with controls. Further details on particular statistical analyses can be found on the respective figures/results section for each data set.

29. Hancock, J. F., Cadwallader, K., Paterson, H. & Marshall, C. J. A CAAX or a CAAL motif and a second signal are sufficient for plasma-membrane targeting of ras proteins. *EMBO J.* **10**, 4033–4039 (1991).



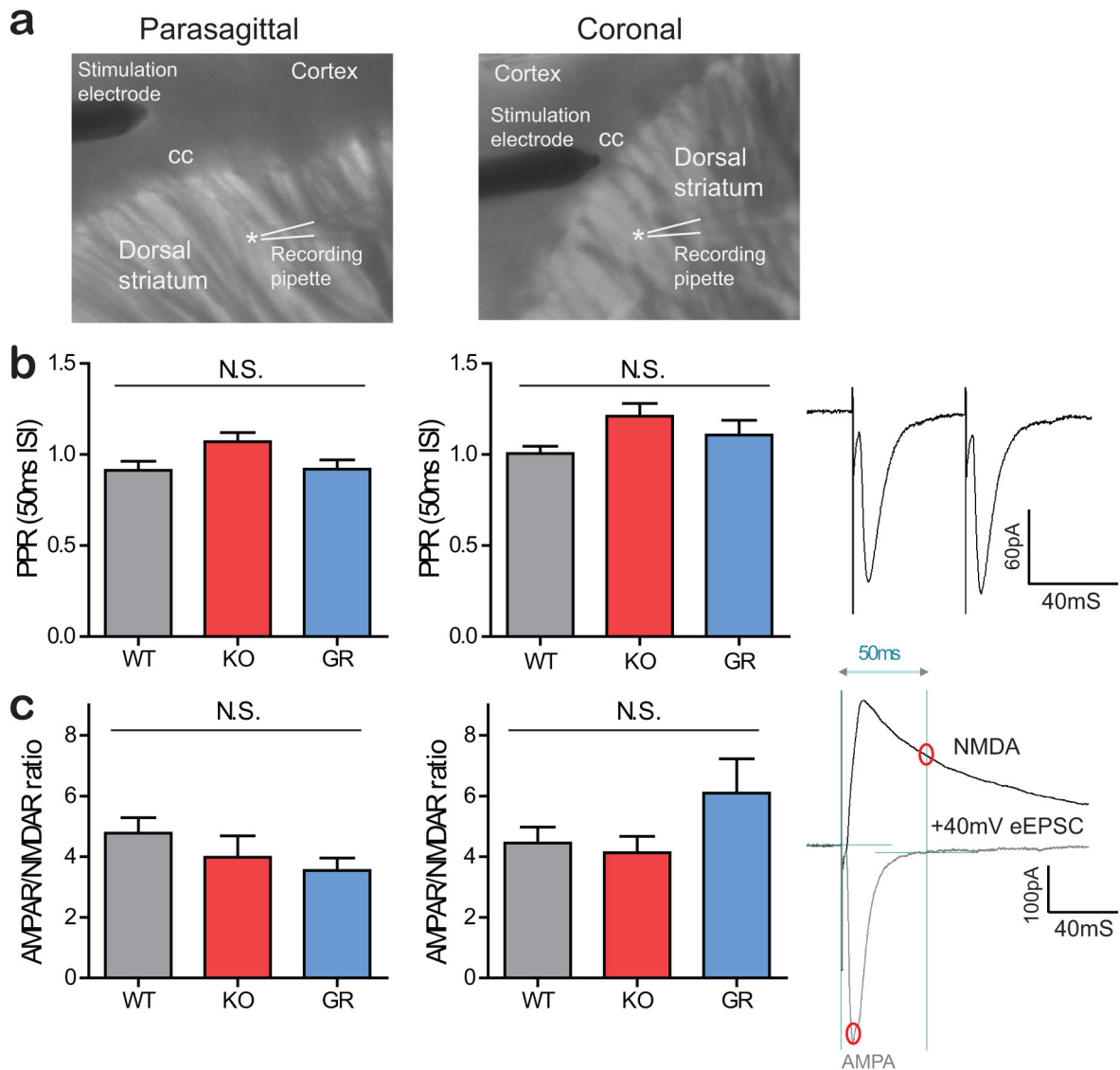
Extended Data Figure 1 | Generation of *Shank3* conditional knock-in mice. **a, i–ii,** Schematic of the *Shank3* gene and the target locus. **a, iii,** Targeted exons 13–16. **a, iv,** Neo-cassette excision via breeding with germline Flp mice. **a, v,** Exons 13–16 re-inversion via Cre-expressing mice. **b,** PCR genotyping showing the bands for Fx (knockout), rescue and WT. **c,** Western blot showing rescue of *Shank3* expression upon germline Cre recombination, with the exception of the putative SHANK3 γ isoform. This is probably due to the disruption of a putative intronic promoter by

the introduction of the *loxP* sites. **d,** Tamoxifen-inducible Cre strategy leads to broad reporter expression. Sagittal sections from pCAGGS-CreER^{+/−}:Rosa-floxstop-tdTomato^{+/−} mice after feeding with tamoxifen (left) or corn oil (right). Results show widespread induction of tdTomato reporter expression after tamoxifen-induced Cre activation, but not in the absence of Cre activity (corn oil feeding); the pCAGGS promoter consists of the CMV early enhancer with chicken β -actin promoter¹⁹. See Supplementary Fig. 1 for gel source data.



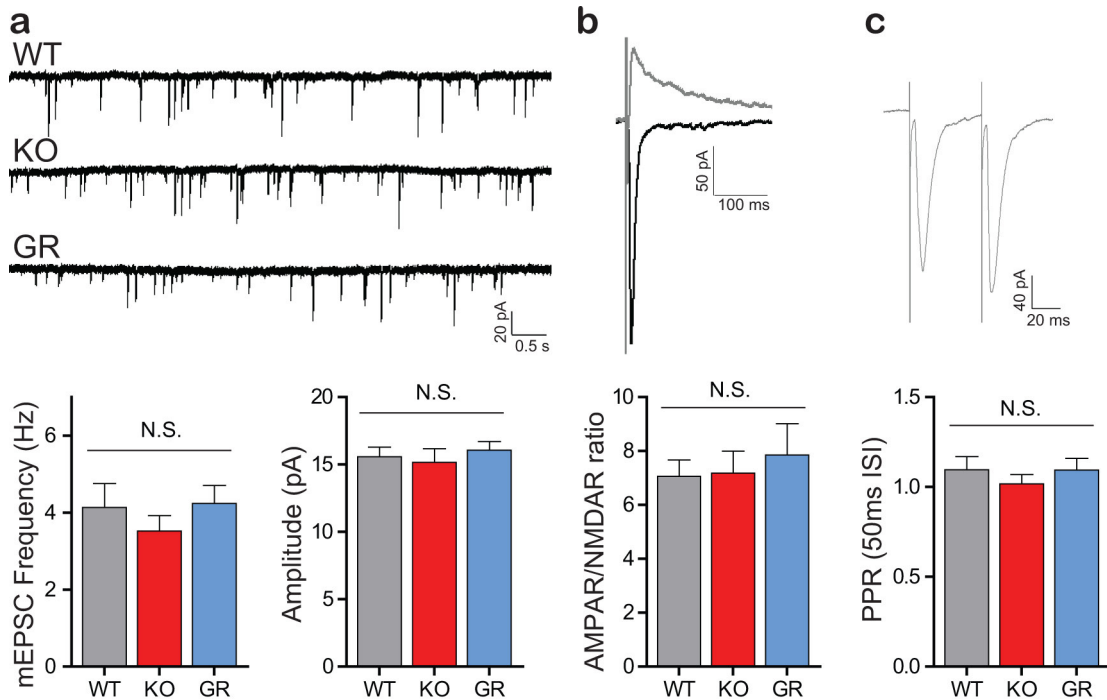
Extended Data Figure 2 | Additional measurements of dorsal striatum synaptic function in TM rescue. **a**, Representative traces (left) and bar graph (right) for the AMPAR/NMDAR ratio in WT, KO and TM groups ($n = 30$ WT, $n = 33$ KO and $n = 33$ TM MSNs). AMPAR/NMDAR ratio calculated as the ratio of the EPSC peak amplitude at -70 mV (AMPA EPSC) to the amplitude of the EPSC recorded at $+40$ mV, 50 ms after afferent stimulation. **b**, Representative traces (left) and bar graph (right) for pharmacologically isolated AMPAR/NMDAR ratio ($n = 20$ WT,

$n = 20$ KO and $n = 23$ TM MSNs). Dual-component evoked EPSC at $+40$ mV recorded before and after AP5 bath application. **c**, Representative traces (left) and bar graph (right) for the NR2B/NMDAR ratio in WT, KO and TM groups ($n = 16$ WT, $n = 16$ KO and $n = 22$ TM MSNs). Dual-component evoked EPSC at $+40$ mV recorded before and after ifenprodil bath application. N.S., not significant (Kruskal–Wallis test, with Dunn's multiple comparison test (a), one-way ANOVA with Bonferroni post-hoc test (b, c)). Data are mean \pm s.e.m.



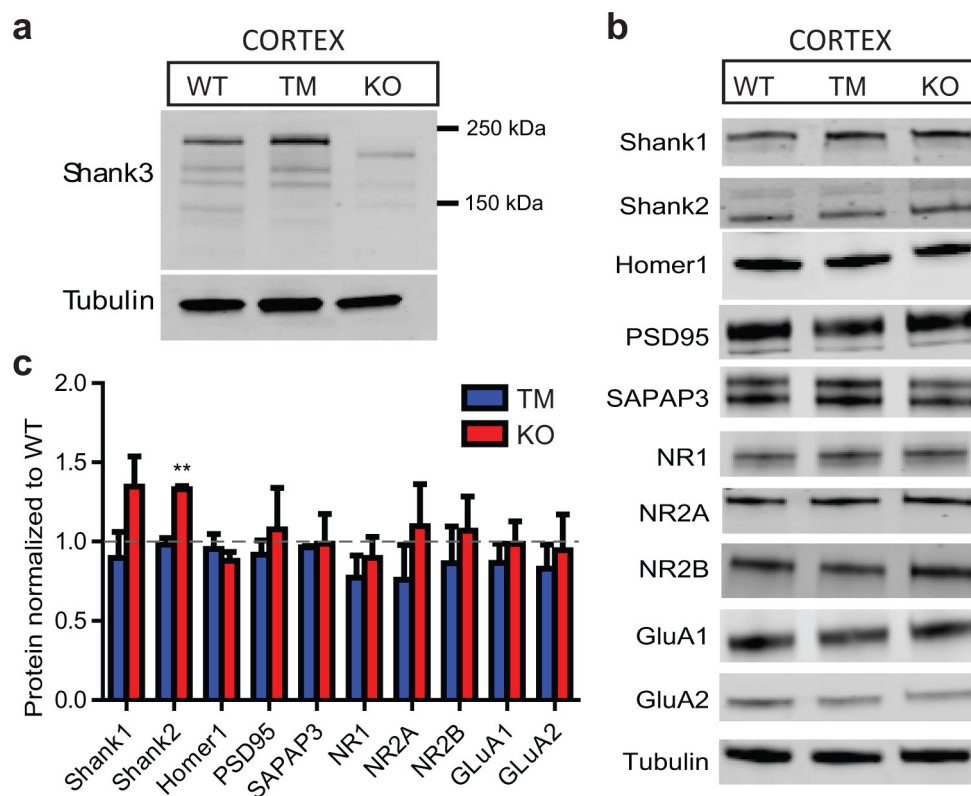
Extended Data Figure 3 | Additional measurements of synaptic function in dorsal striatum by cortical and corpus callosum evoked stimulation. **a**, IR-DIC images showing representative placement of the stimulation electrode in the cortex (left) or corpus callosum (cc; right) to evoke EPSCs in dorsal striatum, using parasagittal (left) and coronal (right) slices. **b**, Representative traces (right) and summary bar graphs for the paired-pulse ratios (PPR) of evoked EPSCs in dorsal striatum MSNs, showing similar magnitude in parasagittal (left; $n = 23$ WT, $n = 20$ KO and $n = 20$ TM MSNs) and coronal (right; $n = 9$ WT, $n = 11$ KO and

$n = 10$ TM MSNs) slices. One-way ANOVA with Bonferroni post-hoc test. **c**, Representative traces (right) and summary bar graphs of AMPAR/NMDAR ratios evoked in parasagittal (left; $n = 17$ WT, $n = 15$ KO and $n = 16$ TM MSNs) and coronal (right; $n = 20$ WT, $n = 16$ KO and $n = 15$ TM MSNs) slices from all three genotypes. AMPAR/NMDAR ratio calculated as the ratio of the EPSC peak amplitude at -70 mV (AMPA EPSC) to the amplitude of the EPSC recorded at $+40$ mV, 50 ms after afferent stimulation (**c**, right). Kruskal–Wallis test, with Dunn’s multiple comparison test. Data are mean \pm s.e.m.



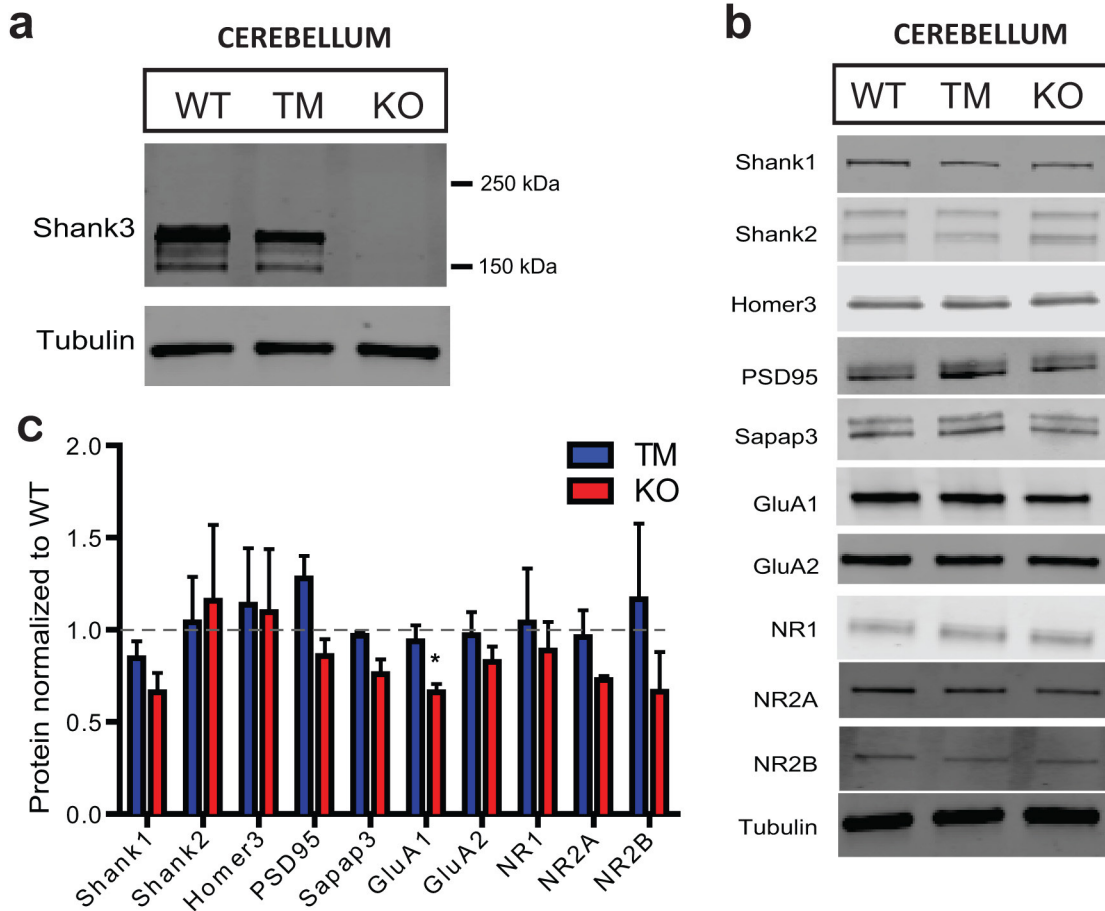
Extended Data Figure 4 | Whole-cell measurements of excitatory synaptic function in nucleus accumbens. **a**, Representative traces (top) and summary bar graphs (bottom) of mEPSCs in nucleus accumbens (NAc) MSNs ($n = 22$ WT, $n = 16$ KO and $n = 18$ GR MSNs). **b**, Representative traces (top) and summary bar graph (bottom) of the AMPAR/NMDAR ratio in NAc MSNs. The AMPAR/NMDAR ratio was calculated as the ratio of the EPSC peak amplitude at -70 mV (AMPA

EPSC) to the amplitude of the EPSC recorded at $+40$ mV, 50 ms after afferent stimulation ($n = 19$ WT, $n = 16$ KO and $n = 15$ GR MSNs). **c**, Representative traces (top) and summary bar graph (bottom) of paired-pulse ratios in NAc MSNs ($n = 25$ WT, $n = 22$ KO and $n = 19$ GR MSNs). One-way ANOVA Bonferroni post-hoc test (**a**, **c**), Kruskal-Wallis test, with Dunn's multiple comparison test (**b**). Data are mean \pm s.e.m.



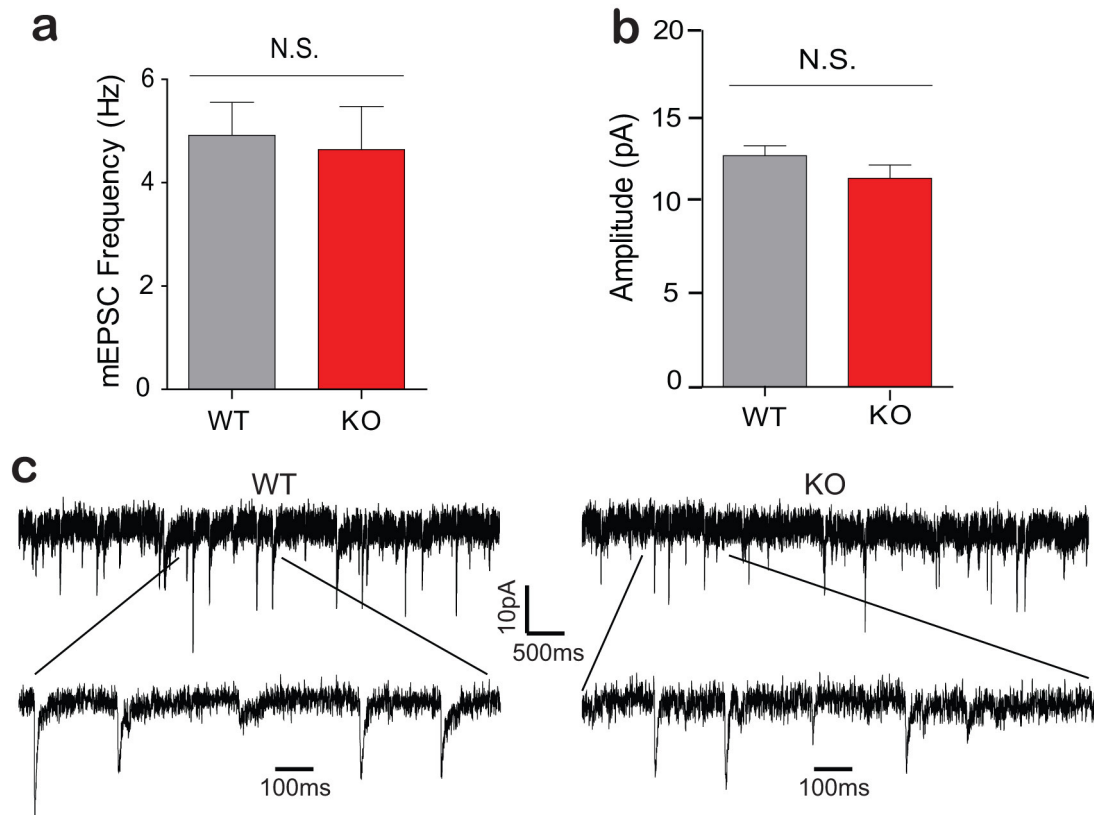
Extended Data Figure 5 | Western blots of synaptosomal preparations from the cortex of the adult treated mice show minimal difference across genotypes. **a**, Representative western blot of SHANK3 in the cortex of adult WT, KO and TM mice, showing that most major SHANK3 isoforms are restored in the TM mice. **b**, Representative western blots of synaptic proteins including scaffolding proteins and neurotransmitter

receptors in the adult cortex across genotypes. **c**, Quantification of multiple synaptic proteins in the cortex of the adult treated mice. All data, $n = 3$ WT, $n = 3$ TM and $n = 3$ KO mice; each sample is from tissue taken from two animals. Student's two-tailed unpaired t -test. Data are mean \pm s.e.m. See Supplementary Fig. 1 for gel source data.



Extended Data Figure 6 | Western blots of synaptosomal preparations from the cerebellum of the adult treated mice show minimal difference across genotypes. **a**, Representative western blot of SHANK3 in the cerebellum of the adult mice treated with TM, showing that SHANK3 isoforms are restored in the TM mice. **b**, Representative western blots of synaptic proteins in the adult cerebellum across genotypes.

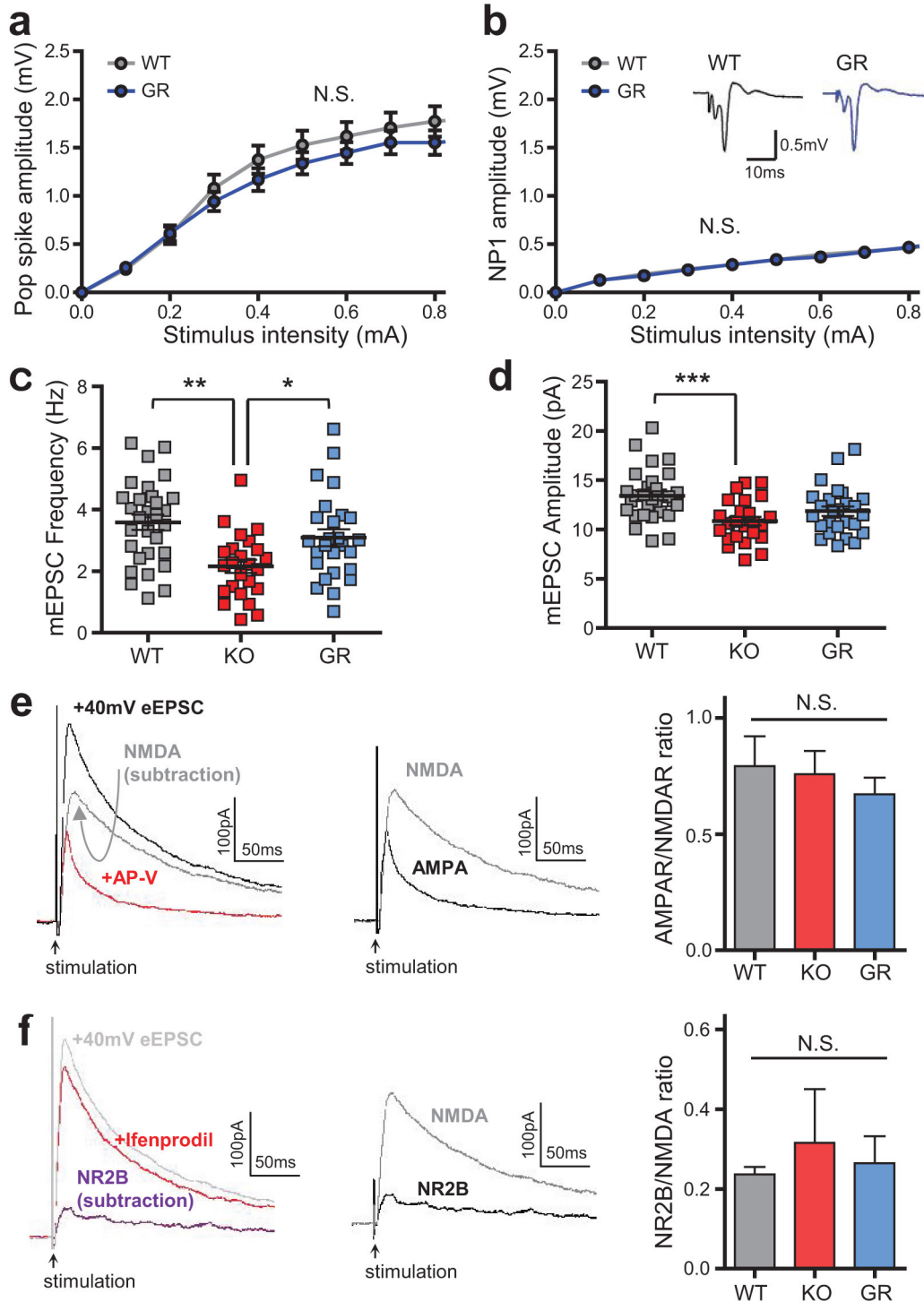
c, Quantification of multiple synaptic proteins in the cerebellum of the adult treated mice. All data, $n = 3$ WT, $n = 3$ TM and $n = 3$ KO mice; each sample is from tissue taken from a single animal. Student's two-tailed unpaired *t*-test. Data are as mean \pm s.e.m. See Supplementary Fig. 1 for gel source data.



Extended Data Figure 7 | Whole-cell measurements of excitatory synaptic function in the cortex. **a, b**, Summary bar graphs of mEPSC frequency (**a**) and amplitude (**b**) in the prefrontal cortex of the adult

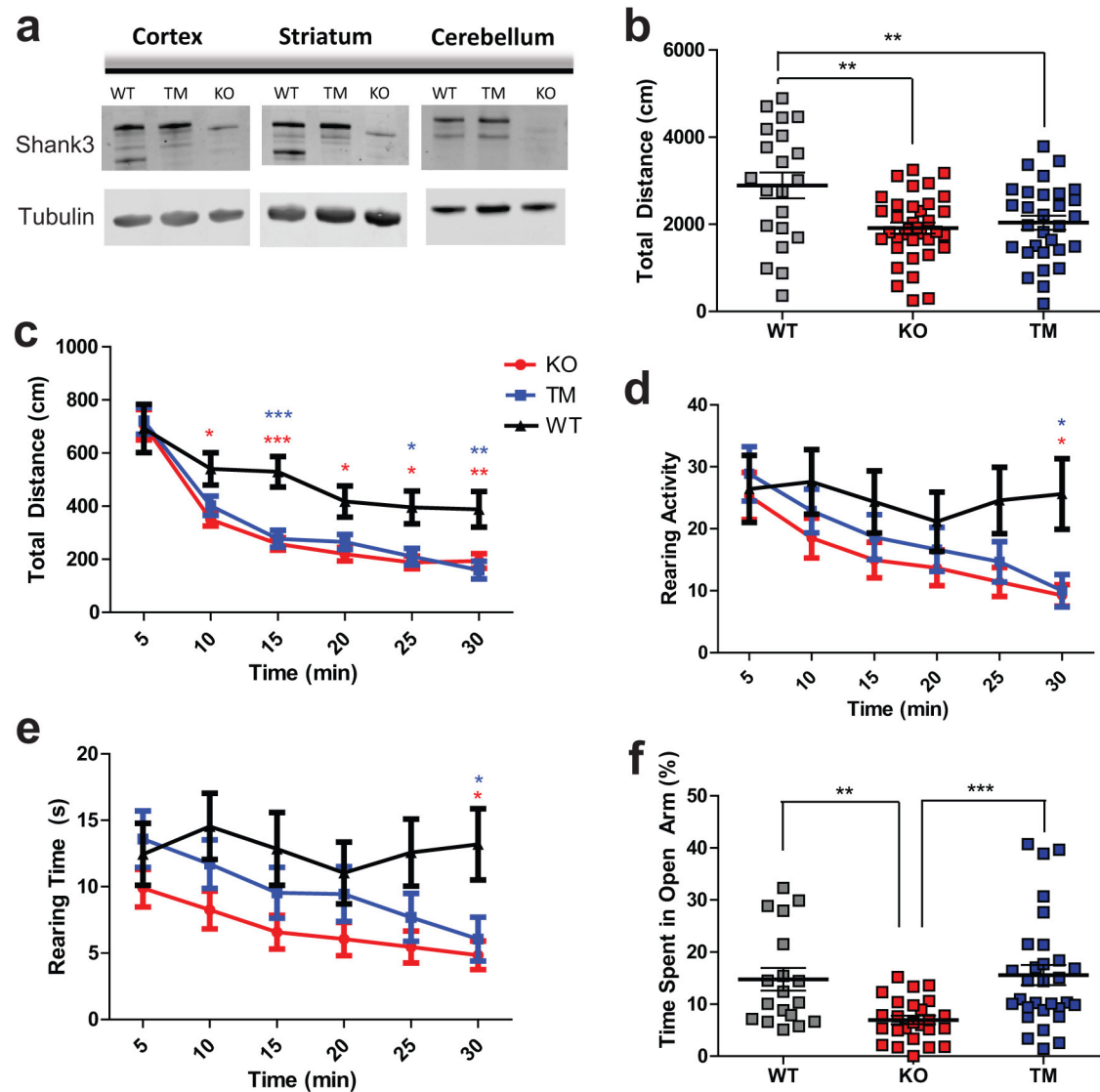
WT and KO mice ($n = 13$ WT and $n = 10$ KO cells; Student's two-tailed unpaired t -test). Data are mean \pm s.e.m. **c**, Representative traces from mEPSC recordings in the adult prefrontal cortex of the WT and KO mice.

GERMLINE



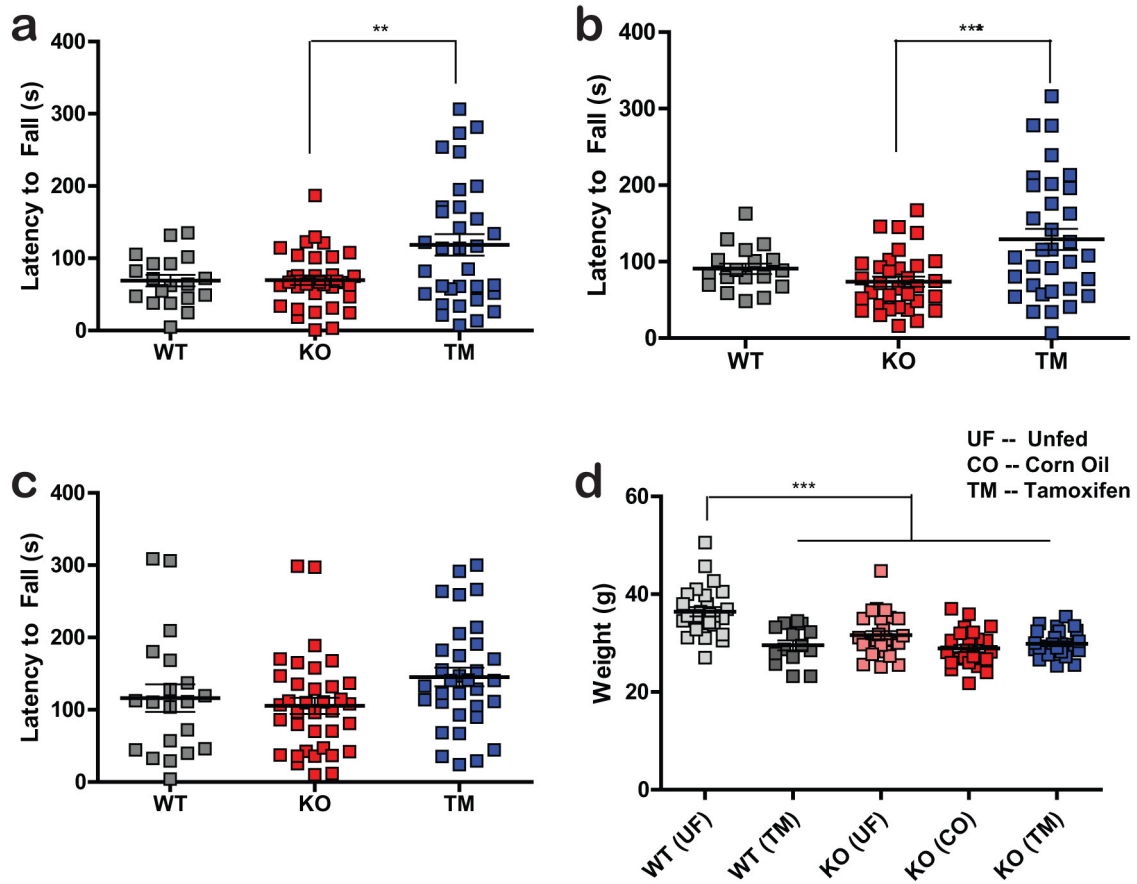
Extended Data Figure 8 | Electrophysiological measurements in the dorsal striatum of germline rescue mice. **a, b**, Normal pop spike amplitude (**a**) and NP1 (**b**) in germline rescued mice (insets show representative field traces). **c, d**, Reduced mEPSC frequency in KO compared to WT and GR mice (**c**). A reduction in mEPSC peak current amplitude is observed between KO and WT group only (**d**) ($n = 30$ WT, $n = 24$ KO and $n = 26$ GR MSNs). **e**, Representative traces (left) and bar graph (right) for the pharmacologically isolated AMPAR/NMDAR ratio

($n = 9$ WT, $n = 9$ KO and $n = 8$ GR MSNs). Dual-component evoked EPSC at +40 mV recorded before and after DL-AP5 bath application. **f**, Representative traces (left) and bar graph (right) for NR2B/NMDAR ratio in WT, KO and GR groups ($n = 6$ WT, $n = 5$ KO and $n = 7$ GR MSNs). Dual-component evoked EPSC at +40 mV recorded before and after ifenprodil bath application. * $P < 0.05$; ** $P < 0.01$; *** $P < 0.001$ (two-way (**a, b**) and one-way (**c-f**) ANOVA with Bonferroni post-hoc test). Data are mean \pm s.e.m.



Extended Data Figure 9 | Expression of SHANK3 at P20–P21 rescues some behavioural measurements. **a**, Representative western blots showing efficient SHANK3 re-expression in the cortex, striatum and cerebellum in mice that were treated with tamoxifen at P20–P21. **b**, The total distance travelled as measured by the open-field test was not improved in the TM condition compared to the KO condition. One-way ANOVA with Bonferroni post-hoc test. **c**, The open-field total distance plotted across 5-min time bins, showing that there is no difference between KO and TM conditions across time. **d**, Rearing activity measured by open-field plotted across time, showing that the TM mice perform

in between the WT and KO mice for most of the 30-min test. **e**, Rearing time measured by open-field test plotted across time, also showing the intermediate performance of TM mice between that of WT and KO mice (**b–e**: $n = 21$ WT, $n = 36$ KO and $n = 30$ TM mice; two-way ANOVA with Bonferroni post-hoc test). **f**, Activity on the zero maze indicates that the TM condition shows significantly reduced anxiety compared to that of the KO condition ($n = 18$ WT, $n = 25$ KO and $n = 30$ TM mice; outliers were removed using Iglewicz and Hoaglin's test (two-sided); Kruskal–Wallis test, Dunn's multiple comparison test). Data are mean \pm s.e.m. See Supplementary Fig. 1 for gel source data.



Extended Data Figure 10 | Expression of SHANK3 at P20–P21 improves motor coordination. **a**, Summary data from trial 1 of the accelerating rotarod test on mice treated with TM at P20–P21 ($n = 19$ WT, $n = 35$ KO and $n = 33$ TM mice). **b**, Summary data from trial 2 of the same rotarod test on mice treated at P20–P21 ($n = 18$ WT, $n = 33$ KO and $n = 33$ TM mice). **c**, Summary data from trial 3 of the rotarod on mice treated at P20–P21 ($n = 20$ WT, $n = 36$ KO and $n = 33$ TM mice). Outliers in

a–c were removed using Iglewicz and Hoaglin's robust outlier test. One-way ANOVA with Bonferroni post-hoc test. **d**, Body weight from WT and KO mice that were unfed (UF) and mice that were fed with either corn oil or TM ($n = 28$ WT (UF), $n = 14$ WT (TM), $n = 27$ KO (UF), $n = 25$ KO (CO) and $n = 26$ KO (TM)). One-way ANOVA with Bonferroni post-hoc test. Data are mean \pm s.e.m.